scientific reports

Check for updates

OPEN

Uncovering upconversion photoluminescence in layered PbI_2 above room temperature

Sharad Ambardar[1], Xiaodong Yang[2] & Jie Gao[1]✉

As a van der Waals (vdW) layered semiconductor material, lead iodide (PbI_2) possessing a direct bandgap with strong photoluminescence emission in visible range has gained wide attention in applications of photonic and optoelectronic devices. Here, upconversion photoluminescence (UPL) in exfoliated PbI_2 flakes is demonstrated at room temperature and elevated temperatures. The linear power dependence of UPL emission with 532 nm excitation suggests the one-photon involved multiphonon-assisted UPL emission process, which is revealed by the temperature-dependent UPL emission measurement. Meanwhile, the nonlinear power dependence of UPL emission with 561 nm excitation indicates the transition of UPL emission mechanism from linear to nonlinear regime, and the temperature-dependent UPL emission study further shows that the upconversion is contributed by both the multiphonon-assisted UPL process and the two-photon absorption induced PL process. This study will provide an insight to the understanding of photon upconversion in vdW layered semiconductors and advancing applications in temperature-controlled photon upconversion, tunable photonics, photodetection and imaging.

Keywords Upconversion photoluminescence, Layered PbI_2

Upconversion photoluminescence (UPL) is an anti-Stokes physical process where the energy of the emitting photons is higher than that of the absorbed photons, which is contrary to the downconversion process that obeys Stokes' law. The additional upconversion energy can be achieved due to different mechanisms such as phonon participation[1–3], multiphoton absorption[4–6], triple-triplet annihilation[5], and Auger recombination[7]. During the UPL emission process, low-energy excitation photons couple with real or virtual intermediate states such as surface states, defect states or electronic subbands[8–12]to generate high-energy states, which lead to the emission of photons with upconversion energy gain[13,14]. In particular, phonon-assisted UPL is gaining a lot of interest since it is a one-photon involved linear process with upconversion energy gain compensated by multiphonon absorption, which is distinct from the nonlinear two-photon absorption induced PL process. UPL phenomena possess a broad area of applications such as photovoltaics[5,15], lasers[16], optical refrigeration[17,18], and optical tweezers[19]. UPL processes can be realized in various material systems especially in low-dimensional materials such as 2D materials and their heterostructures[20–26], quantum wells[27]and quantum dots[28], nanobelts[29], and carbon nanotubes[12].

Since the last two decades, van der Waals (vdW) layered materials have gained tremendous interest due to their exceptional properties and wide applications in optoelectronics[30–32], spintronics[33]and valleytronics[34]. Additionally, 2D layered materials possess tunable bandgap in a wide range upon varying the thickness, which make them excellent candidates in developing flexible devices[35,36], field effect transistors[37,38], and photodetectors[39,40]. One such layered semiconductor material is lead iodide (PbI_2) from the group of transition metal halides, which has shown a great potential for applications such as nuclear radiation detectors[41,42], perovskite fabrication[43,44], photodetectors[45,46], and nanolasers[47]. Similar to monolayer transition metal dichalcogenides (TMDs), layered PbI_2exhibits a direct bandgap around 2.4 eV and strong photoluminescence emission in the visible[48–51], which makes it an excellent 2D material for excitonic physics and device studies. Recently, PL and UPL emission in PbI_2at low temperatures have been studied[25,52–54], but the UPL emission of layered PbI_2 above room temperature has not been explored yet, and the roles of phonon-assisted upconversion process and two-photon absorption upconversion process are not well understood.

In this work, upconversion photoluminescence emission in mechanically exfoliated layered PbI_2 flake is demonstrated at room temperature and elevated temperatures using continuous-wave laser excitation. The

[1]Department of Mechanical Engineering, Stony Brook University, Stony Brook NY11794, USA. [2]Department of Mechanical and Aerospace Engineering, Missouri University of Science and Technology, Rolla, MO 65409, USA. ✉email: jie.gao.5@stonybrook.edu

linear excitation power dependence of UPL emission under 532 nm excitation is observed at room temperature, which suggests the one-photon involved multiphonon-assisted UPL emission process in the linear regime. The nonlinear excitation power dependence of UPL emission under 561 nm excitation is obtained, which indicates the transition of UPL emission mechanism from one-photon linear regime to a nonlinear regime with the two-photon absorption induced PL process. It is shown that the temperature-dependent UPL emission under 532 nm excitation follows the multiphonon-assisted UPL process with the upconversion energy gain varying from 98 meV to 77 meV. On the other hand, the temperature-dependent UPL emission under 561 nm excitation is contributed by both the multiphonon-assisted UPL process and the two-photon absorption induced PL process with the upconversion energy gain varying from 209 meV to 184 meV, while the contribution of phonon-assisted UPL process increases with the temperature. With the growing interest in vdW layered semiconductors, the demonstrated results of UPL emission in layered PbI_2 will pave the way for more understanding of photon upconversion in layered semiconductors and assist in broadening its applications in temperature-controlled photon upconversion, tunable photonics, photodetection and imaging.

Results and discussion

As shown by the schematics in Fig. 1(a), the crystal structure of 2D layered $PbI_2$is arranged as a hexagonal lattice[51], where one layer of lead atoms is sandwiched between two layers of iodine atoms and the layers are covalently bonded to each other. The adjacent PbI_2 layers are stacked together by weak van der Waals forces. PbI_2 flakes are mechanically exfoliated from the bulk PbI_2 crystal onto a quartz substrate. Figure 1(b) shows the optical microscope image of one typical exfoliated PbI_2 flake. The atomic force microscopy (AFM) image of the flake is shown in Fig. 1(c), and the height profile indicates that the flake thickness is around 150 nm. PbI_2 flakes exhibit strong excitonic PL emission due to its direct bandgap around 2.4 eV. Figure 1(d) displays the measured Raman spectrum of the exfoliated PbI_2flake with 632.8 nm excitation. Three pronounced Raman peaks at 98 cm^{-1}, 111 $cm^{-1}$and 168 cm^{-1} are observed, which are attributed to A_{1g}, A_{2u} and $2E_g$ modes, respectively[55,56].

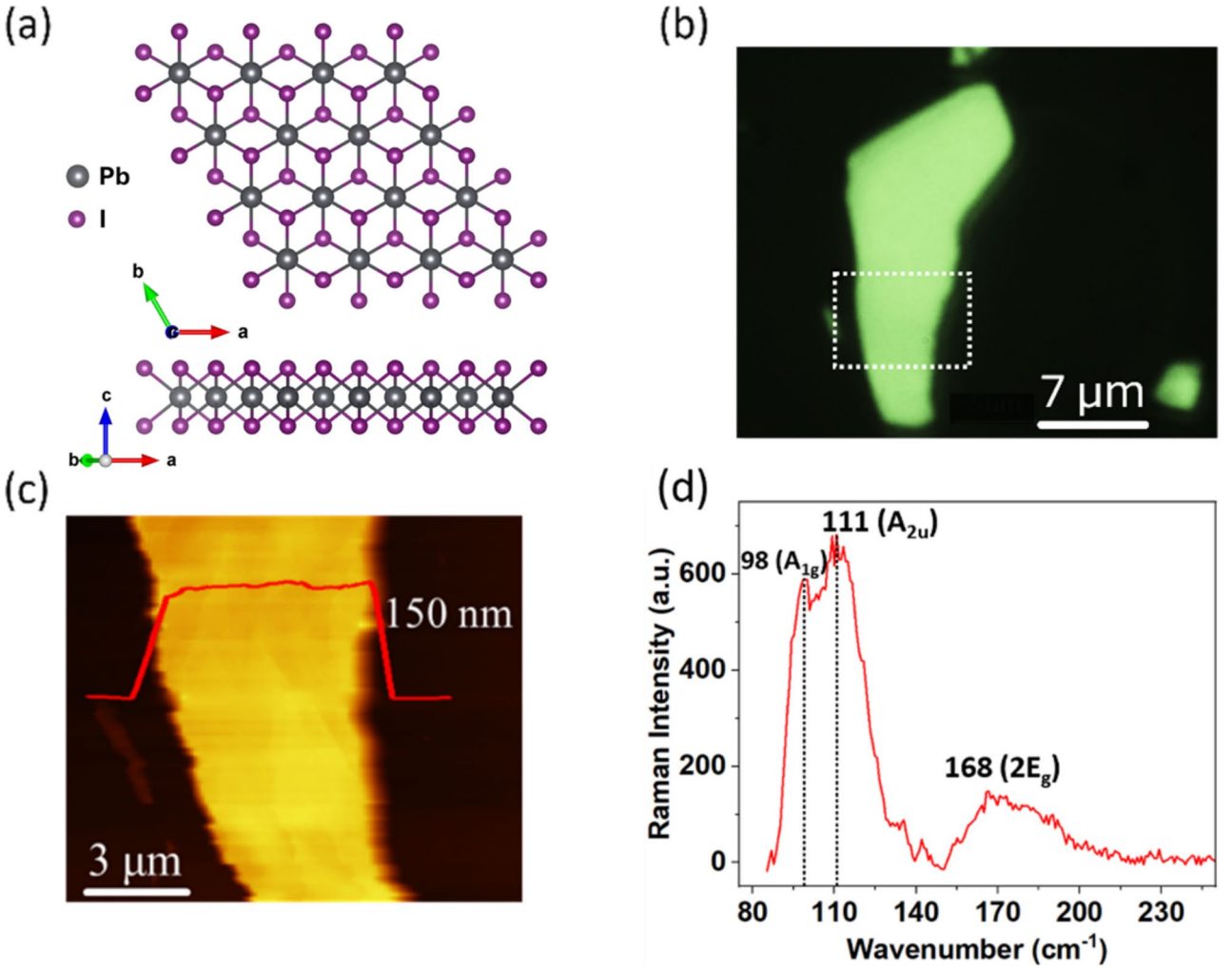

Fig. 1. (**a**) Schematic diagram of PbI_2 crystal structure. (**b**) Optical microscope image of one mechanically exfoliated PbI_2 flake on quartz substrate. (**c**) AFM image of the flake area marked by the white dotted lines in (**b**), indicating the flake thickness of 150 nm. (**d**) Measured Raman spectrum of the PbI_2 flake.

The symmetric stretching of two iodine atoms is responsible for the A_g modes. The A_{2u} mode represents the stretching of two iodine atoms in the same direction with lead atom vibrating in the opposite direction. Additionally, the broad $E_g$mode is due to the shearing motion of two iodine layers[57].

Figure 2(a) shows the measured room-temperature PL and UPL spectra excited by continuous-wave lasers at the wavelength of 445 nm with the excitation power of 60 μW and the integration time of 7 s, 532 nm with 1.48 mW and 10 s, and 561 nm with 9.18 mW and 20 s, respectively. The PL and UPL spectra are fitted by the Voigt fitting as shown with the dashed lines. The UPL emission peak wavelengths are around 515 nm, which is very close to that of the PL emission at 512 nm. The UPL peak intensity per unit power per unit integration time excited at 532 nm is about 78 times stronger than that of 561 nm, while being around 59 times weaker than the PL peak intensity excited at 445 nm. For the PL emission process of PbI_2 flakes, excitons generated with the above-bandgap excitation at the energy of 2.79 eV will relax to the band edge and lead to the excitonic photon emission with the radiative recombination at the energy of 2.42 eV. On the contrary, the excitonic UPL emission occurs when the excitation energy is below the bandgap. As shown in Fig. 2(b) and (c), there are two possible distinguished mechanisms governing the UPL emission, which are one-photon involved multiphonon-assisted upconversion PL process and two-photon absorption induced PL process. As depicted in Fig. 2(b), the multiphonon-assisted UPL process involves the coupling of multiple phonons from the lattice to an intermediate state followed by the relaxation to the band edge to generate the excitonic emission while momentum and energy are conserved during the upconversion emission process[2,3,9]. The phonon-assisted upconversion PL has a linear excitation power dependence due to the one photon absorption. On the other hand, two-photon absorption induced PL process as shown in Fig. 2(c) represents the photon upconversion mechanism excited by the simultaneous absorption of two low-energy photons via a virtual intermediate state and then followed by the spontaneous excitonic emission from the excited state[58–60]. Two-photon absorption is a nonlinear optical process typically with a smaller absorption cross section than the one-photon absorption case. The efficiency of two-photon absorption induced upconversion is usually low and the emission is proportional to the square of the excitation intensity.

The excitation power-dependent PL and UPL spectra at room temperature are measured at the excitation wavelength of 445 nm, 532 nm and 561 nm, as shown in Fig. 3(a), (c) and (e). It is noticed that the emission intensities for all three excitation wavelengths go up with the increased excitation power while maintaining the spectral profile shape. Only the partial range of UPL spectra below 523 nm is included in Fig. 3(c) at the excitation wavelength of 532 nm due to the wavelength cutoff by a 532 nm shortpass filter, while the full range of UPL spectra is provided in Fig. 3(e) at the excitation wavelength of 561 nm when a 546 nm shortpass filter is used. Figure 3(b), (d) and (f) show the integrated PL and UPL intensity as a function of laser excitation power in a log-log scale at each excitation wavelength, respectively. It is observed that the integrated intensity follows a power law of $I = \alpha P^{\beta}$, where P is the excitation power, α is the fitting parameter, and β is the exponent that represents the slope of the curve. The value of β can be used to determine the distinguished mechanisms responsible for the UPL emission process at room temperature as illustrated in Fig. 2(b) and (c). The fitted value of β around 1.12 ± 0.02 in Fig. 3(b) indicates the as-expected linear excitation power dependence for the PL emission excited using a continuous-wave 445 nm laser. In the case of the UPL process excited at 532 nm shown in Fig. 3(d), the linear power dependence with the value of β around 1.04 ± 0.02 suggests the one-photon involved multiphonon-assisted upconversion PL emission process in the linear regime, in which the excitonic emission at the band edge of PbI_2 crystal with the below-bandgap photon excitation is mediated by absorbing

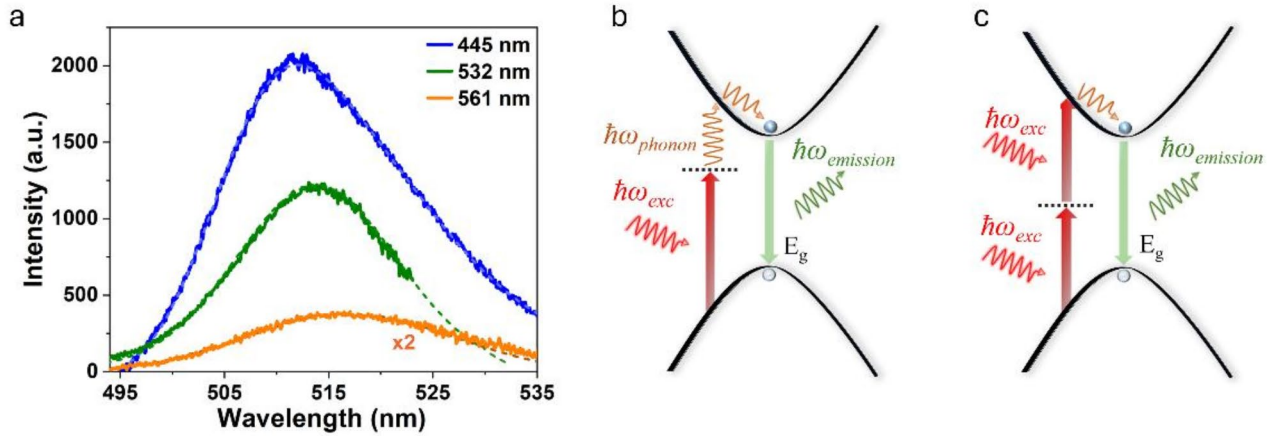

Fig. 2. (**a**) PL and UPL spectra of the PbI_2 flake at excitation wavelengths of 445 nm (blue), 532 nm (green) and 561 nm (orange). (**b**) Schematic illustration of the underlying mechanism responsible for phonon-assisted upconversion PL process, where phonons are coupled to an intermediate state followed by the relaxation to the band edge to generate the excitonic emission while momentum and energy are conserved. (**c**) Schematic illustration of the underlying mechanism responsible for two-photon absorption induced PL process, where the simultaneous absorption of two low-energy photons via a virtual intermediate state is presented and then followed by the spontaneous excitonic emission from the excited state in a nonlinear optical process.

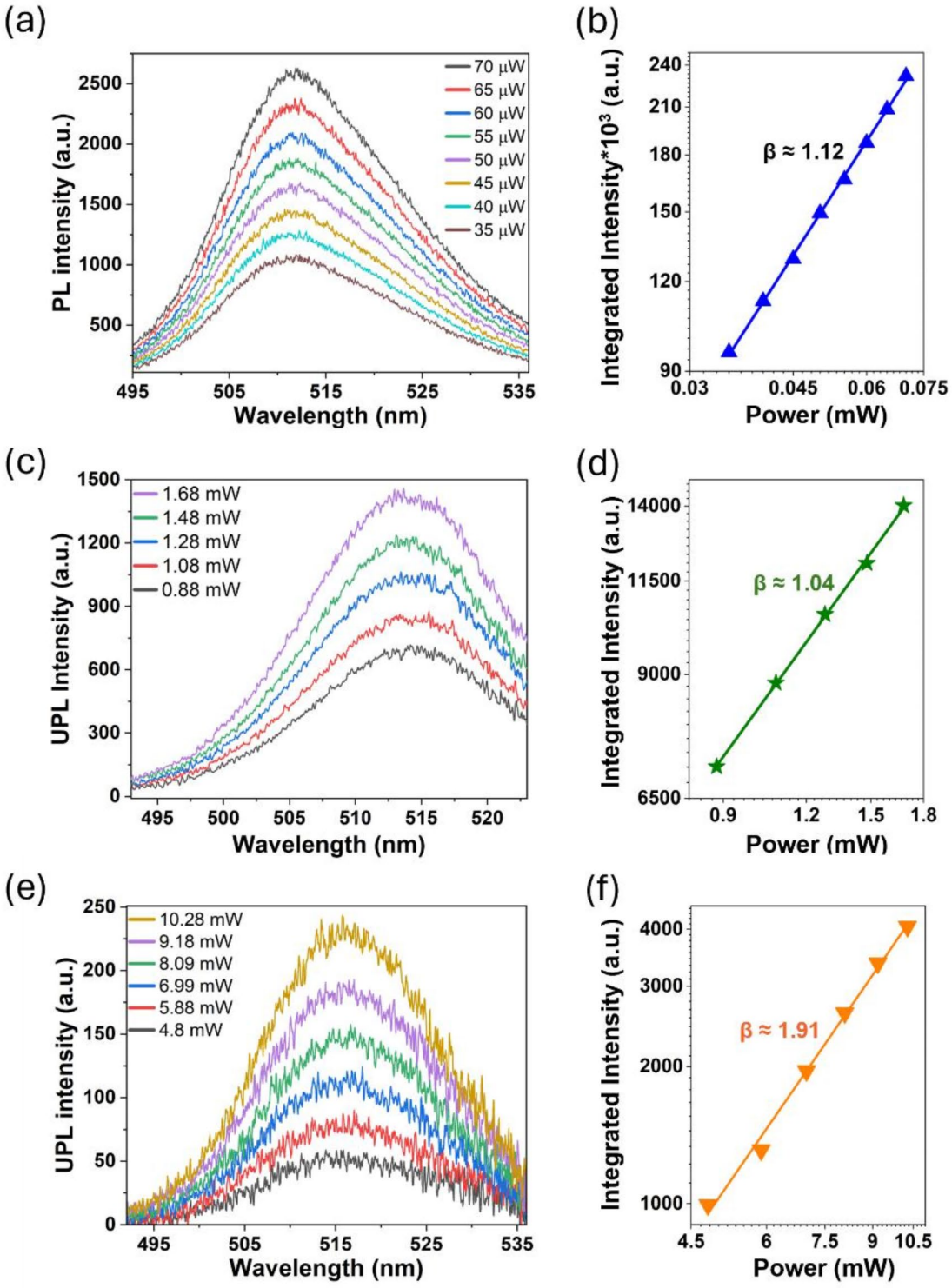

Fig. 3. Measured excitation power-dependent PL and UPL spectra at room temperature excited at the wavelength of (**a**) 445 nm (**c**) 532 nm and (**e**) 561 nm. Integrated PL and UPL intensity as a function of excitation power in a log-log scale for (**b**) 445 nm, (**d**) 532 nm and (**f**) 561 nm excitation. The measured data are presented by the solid dots and the data fittings to the power law are shown as solid lines.

additional energy from multiple phonons. Such additional energy provided by phonons can be defined as the upconversion energy gain $\Delta E = \hbar\omega_{UPL} - \hbar\omega_{exc}$, where $\hbar\omega_{UPL}$ is the energy of upconversion emission photons and $\hbar\omega_{exc}$ is the energy of excitation photons. The upconversion energy gain is due to the contribution of multiphonon absorption process via the transverse optical (TO) phonon of A_{1g} mode with phonon energy around 12 meV in

layered PbI_2. By considering the upconversion energy gain of 81 meV obtained at the excitation wavelength of 532 nm at room temperature, the effective number of phonons involved in the phonon-assisted UPL process in layered PbI_2 is approximately estimated from 6 to 7. As plotted in Fig. 3(f), when the laser excitation wavelength is 561 nm with the power from 4.8 to 10.28 mW (corresponding to excitation irradiance from 0.61 to 1.31 MW/cm^2), a nonlinear excitation power dependence is observed with the value of β around 1.91 ± 0.07, indicating the transition of UPL emission mechanism from one-photon linear regime to a nonlinear regime with the involvement of two-photon absorption induced PL process.

To further understand the UPL emission mechanisms in layered PbI_2 at elevated temperatures, temperature-dependent PL and UPL emission measurements are carried out with a 160 nm-thick PbI_2 flake. A Linkam THMS600 heating stage is used for high-temperature PL and UPL characterizations. Figure 4(a) shows temperature-dependent PL emission spectra from 294 K to 414 K, where a clear redshift in the PL emission peak wavelength and a gradual decrease of the emission intensity are observed with the increased temperature. As shown in Fig. 4(b), a redshift from 509.5 nm to 518.1 nm in the PL emission peak wavelength is observed when the temperature increases from 294 K to 414 K. This temperature-dependent shift of the emission peak energy can be modelled by the modified Varshni equation $E_g(T) = E_g(0) - S\langle\hbar\omega_{AC}\rangle\left[\coth\left(\frac{\langle\hbar\omega_{AC}\rangle}{2k_BT}\right) - 1\right]$, which typically describes the effect of temperature on the semiconductor bandgap $E_g(T)$. Here $E_g(0)$ represents the excitonic transition energy at T = 0 K, the electron-phonon coupling strength is represented by a dimensionless constant S, average acoustic phonon energy involved in electron-phonon interaction is referred by $\langle\hbar\omega_{AC}\rangle$, and $k_B$is the Boltzmann constant[61,62]. It is shown that the measured emission peak wavelengths follow the Varshni equation as indicated by the solid blue line. $\langle\hbar\omega_{AC}\rangle$ is 39 meV for layered PbI_2[63], and the S value obtained from the Varshni fitting is around 2.21 for the PL process. Figure 4(c) plots the integrated PL emission intensity as a function of temperature, and noticeably the PL emission quenches around 3 times as the temperature increases from 294 K to 414 K. The decrease of PL integrated intensity at high temperatures is associated with the thermal quenching of excitons which follows the Arrhenius equation $I_{PL}(T) = I_0/[1 + R\exp(-E_a/k_BT)]$, where I_0 is the PL intensity at T = 0 K, R is the ratio between the nonradiative and radiative recombination rate, and $E_a$is the thermal activation energy responsible for the dissociation of excitons[64,65]. The measured data for integrated PL emission intensity are well fitted by the solid line with R = 710.8 and E_a = 183 meV.

Figure 5(a) displays temperature-dependent UPL emission spectra from 294 K to 344 K with the excitation at 532 nm, where the UPL peak wavelength is also redshifted at high temperatures. Different from the PL process, the UPL emission intensity grows with the temperature increase. The UPL emission peak wavelength is redshifted from 510.6 nm to 514.9 nm as plotted in Fig. 5(b), where the fitted S value is around 2.38 using the modified Varshni equation. The slightly different S values between PL and UPL processes suggest different electron-phonon and phonon-exciton interactions in the temperature-dependent PL and UPL emission in layered PbI_2. A 3-fold increase of the UPL emission integrated intensity is observed as temperature is increased from 294 K to 344 K in Fig. 5(c). For the phonon-assisted UPL process (PUPL) under 532 nm excitation, the temperature-dependent UPL emission intensity is proportional to the Boltzmann function for phonon population of $\exp(-|\Delta E|/k_BT)$. Considering the thermal quenching of excitonic emission, the UPL intensity can be described as $I_{PUPL}(T) \propto \exp(-|\Delta E|/k_BT)/[1 + R\exp(-E_a/k_BT)]$. The upconversion energy gain ΔE changes from 98 meV to 77 meV as temperature increases due to the temperature-dependent redshift of the bandgap. The theoretical fitting of I_{PUPL} shown as the solid line agrees well with the measured data, where the observed trend is attributed to both the reduced energy gain ΔE and the increased k_BT energy.

Figure 6(a) presents the measured UPL emission spectra at temperatures from 294 K to 354 K at the excitation wavelength of 561 nm. Similar to the 532 nm case, the UPL peak wavelength is redshifted and the UPL emission intensity increases at elevated temperatures. In Fig. 6(b), the UPL peak wavelength is redshifted from 512.5 nm to

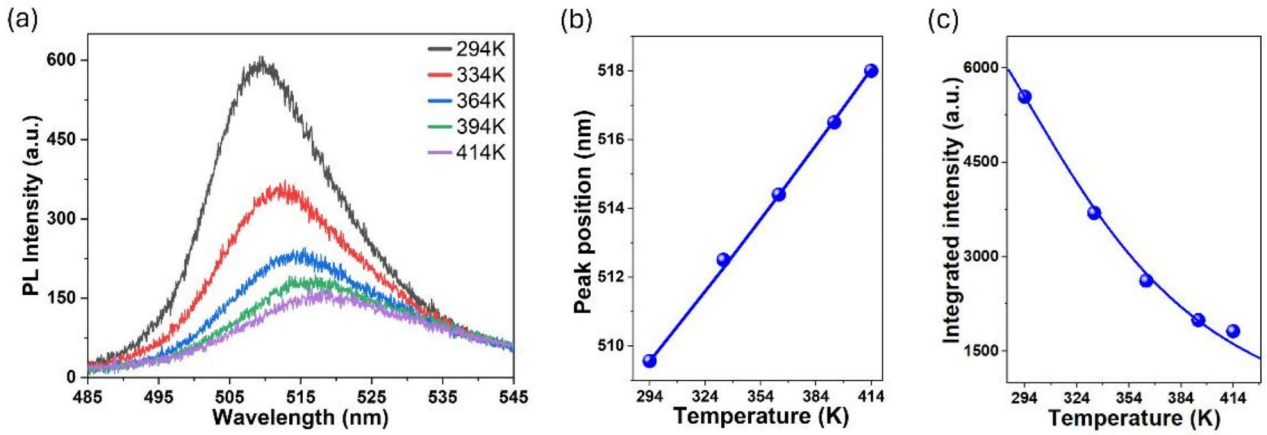

Fig. 4. (**a**) Temperature-dependent PL spectra excited at 445 nm with the excitation power of 40 μW. (**b**) PL emission peak wavelength and (**c**) integrated PL emission intensity as a function of temperature. Experimental measurements are depicted by the solid dots and theoretical fittings are represented by the solid lines.

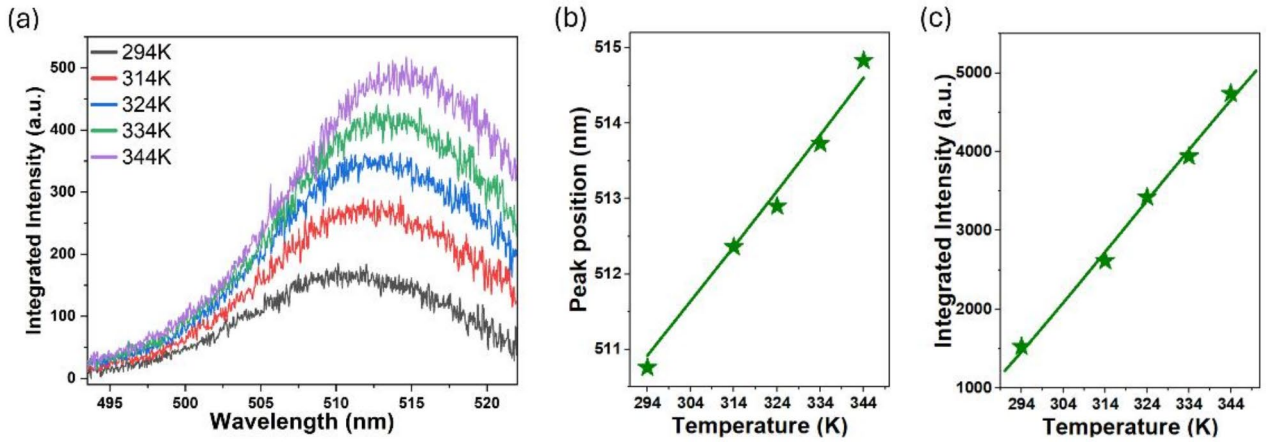

Fig. 5. (**a**) Temperature-dependent UPL spectra excited at 532 nm with the excitation power of 0.8 mW. (**b**) UPL emission peak wavelength and (**c**) UPL emission integrated intensity as a function of temperature. Experimental measurements are depicted by the solid points and theoretical fittings are represented by the solid lines.

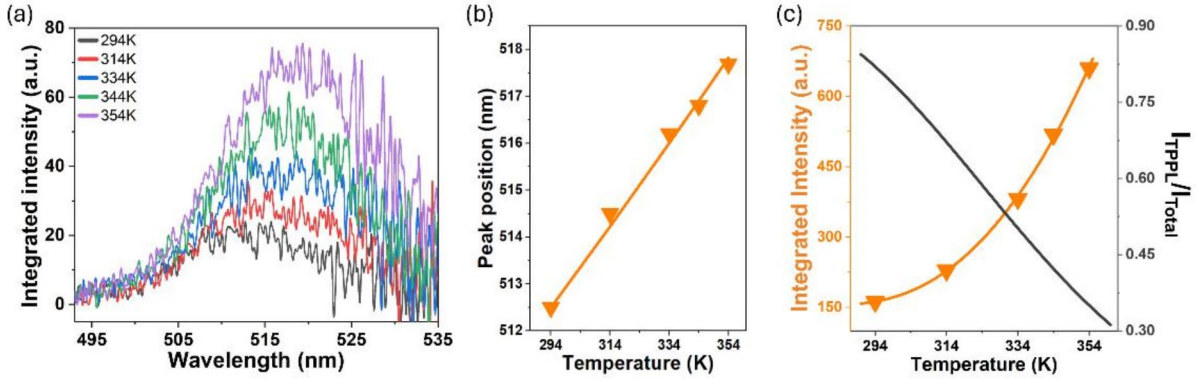

Fig. 6. (**a**) Temperature-dependent UPL spectra excited at 561 nm with the excitation power of 5.6 mW (corresponding to excitation irradiance of 0.71 MW/cm^2). (**b**) UPL emission peak wavelength as a function of temperature. (**c**) UPL emission integrated intensity as a function of temperature. The black solid line depicts the intensity ratio of I_{TPPL} to I_{total}.

517.8 nm, corresponding to the upconversion energy gain ΔE varying from 209 meV to 184 meV. The theoretical fitting shows the S value around 2.89. The UPL emission integrated intensity is increased by more than 4 times with the increased temperature, as observed in Fig. 6(c). For the two-photon absorption induced PL process (TPPL), the emission intensity $I_{TPPL}(T) \propto \beta_2(T)/[1 + R\exp(-E_a/k_BT)]$, where $\beta_2(T) \propto \frac{(2x-1)^{3/2}}{(E_g^3)(2x)^5}$ is the two-photon absorption coefficient with $x = \hbar\omega_{exc}/E_g$[66]. For UPL process under 561 nm excitation, both the phonon-assisted UPL process and the two-photon absorption induced PL process contribute to the observed UPL emission intensity with $I_{total}(T) = I_{PUPL}(T) + I_{TPPL}(T)$. The theoretical fitting of I_{total} plotted as the orange solid line in Fig. 6(c) matches with the measured experimental data points. Additionally, the contribution of the two-photon absorption induced PL process in the photon upconversion emission can be represented by the ratio of I_{TPPL}/I_{total} as shown by the black solid line. It is worth noting that the two-photon absorption induced PL process dominates the UPL emission with the I_{TPPL}/I_{total} ratio of 0.81 at the temperature of 294 K. As the temperature goes up, the contribution of the phonon-assisted UPL process greatly increases so that the I_{TPPL}/I_{total} ratio is reduced to 0.35 at the temperature of 354 K.

Conclusion

In summary, power-dependent and temperature-dependent upconversion photoluminescence in layered PbI_2 has been demonstrated with below-bandgap excitations. The linear excitation power dependence of UPL

emission under 532 nm excitation has been observed at room temperature, suggesting the one-photon involved multiphonon-assisted upconversion PL emission process. The nonlinear excitation power dependence of UPL emission is obtained under 561 nm excitation, indicating the transition of UPL emission mechanism from one-photon linear regime to a nonlinear regime with the involvement of two-photon absorption induced PL process. In addition, the UPL peak wavelength is redshifted and the UPL emission intensity is enhanced at elevated temperatures. It is found that the temperature-dependent UPL emission intensity under 532 nm excitation depends on phonon population and thermal quenching in the multiphonon-assisted UPL process. On the other hand, the temperature-dependent UPL emission under 561 nm excitation is attributed to both the multiphonon-assisted UPL process and the two-photon absorption induced PL process, with the contribution of phonon-assisted UPL process greatly increases as the temperature goes up. The demonstrated results of UPL emission in layered PbI_2 will advance many applications such as photon upconversion devices, thermally tunable photonics, photodetection and imaging.

Methods

Sample preparation

High-quality PbI_2 crystals are synthesized with the float zone technique by 2D Semiconductors. PbI_2 flakes are obtained by mechanically exfoliating bulk PbI_2 crystal using scotch tape (3M tape) followed by repetitive sticking of these exfoliated crystals on a fresh scotch tape. These obtained thin flakes are transferred onto a clean quartz substrate. The PbI_2 flake is covered with a PMMA (950 PMMA A7) encapsulation layer to ensure sample stability in the ambient environment.

Optical measurements

The Raman, PL and UPL spectra are characterized by collecting the back reflected signal from a 50 × objective lens (NA = 0.42) that is coupled into a spectrometer (Horiba iHR 550) through a beam splitter and an edgepass filter. A 633 nm ultrasteep longpass filter is used for Raman spectrum measurement, a 475 nm longpass filter is used for PL spectrum measurement, and a shortpass filter of 532 nm or 546 nm is used for UPL spectrum measurements excited at 532 nm or 561 nm, respectively. The range of laser excitation power is also chosen carefully at low levels to avoid any laser heating induced decomposition of the PbI_2 flake.

Data availability

The datasets generated during and/or analyzed during the current study are available from the corresponding author on reasonable request.

Received: 8 August 2024; Accepted: 31 October 2024
Published online: 06 November 2024

References

1. Sheik-Bahae, M. & Epstein, R. I. Optical refrigeration. *Nat. Photon.* **1**, 693–699 (2007).
2. Jadczak, J. et al. Room temperature multi-phonon upconversion photoluminescence in monolayer semiconductor WS_2. *Nat. Comm.* **10**, 107 (2019).
3. Jones, A. M. et al. Excitonic luminescence upconversion in a two-dimensional semiconductor. *Nat. Phys.* **12**, 323–327 (2016).
4. Auzel, F. Upconversion and anti-stokes processes with f and d ions in solids. *Chem. Rev.* **104**, 139–174 (2004).
5. Zhao, J., Ji, S. & Guo, H. Triplet–triplet annihilation based upconversion: from triplet sensitizers and triplet acceptors to upconversion quantum yields. *RSC Adv.* **1**, 937–950 (2011).
6. Wu, M. et al. Solid-state infrared-to-visible upconversion sensitized by colloidal nanocrystals. *Nat. Photon.* **10**, 31–34 (2016).
7. Cheong, H. M., Fluegel, B., Hanna, M. C. & Mascarenhas, A. Photoluminescence up-conversion in GaAs / a l_x Ga_{1-x} as heterostructures. *Phys. Rev. B.* **58**, R4254–R4257 (1998).
8. Wang, Q. & Wee, A. T. Photoluminescence upconversion of 2D materials and applications. *J. Phys. : Cond Matt.* **33**, 223001 (2021).
9. Hellmann, R. et al. Low-temperature anti-stokes luminescence mediated by disorder in semiconductor quantum-well structures. *Phys. Rev. B.* **51**, 18053–18056 (1995).
10. Eshlaghi, S., Worthoff, W., Wieck, A. D. & Suter, D. Luminescence upconversion in GaAs quantum wells. *Phys. Rev. B.* **77**, 245317 (2008).
11. Wang, X. et al. Photoluminescence upconversion in colloidal CdTe quantum dots. *Phys. Rev. B.* **68**, 125318 (2003).
12. Akizuki, N., Aota, S., Mouri, S., Matsuda, K. & Miyauchi, Y. Efficient near-infrared up-conversion photoluminescence in carbon nanotubes. *Nat. Comm.* **6**, 8920 (2015).
13. Zhou, B., Shi, B., Jin, D. & Liu, X. Controlling upconversion nanocrystals for emerging applications. *Nat. Nanotechnol.* **10**, 924–936 (2015).
14. Baluschev, S. et al. Up-Conversion fluorescence: noncoherent excitation by sunlight. *Phys. Rev. Lett.* **97**, 143903 (2006).
15. Richards, B. S., Hudry, D., Busko, D., Turshatov, A. & Howard, I. A. Photon Upconversion for Photovoltaics and Photocatalysis: a critical review: Focus Review. *Chem. Rev.* **121**, 9165–9195 (2021).
16. Scheps, R. Upconversion laser processes. *Prog Quantum Electron.* **20**, 271–358 (1996).
17. Ha, S. T., Shen, C., Zhang, J. & Xiong, Q. Laser cooling of organic–inorganic lead halide perovskites. *Nat. Photon.* **10**, 115–121 (2016).
18. Epstein, R. I., Buchwald, M. I., Edwards, B. C., Gosnell, T. R. & Mungan, C. E. Observation of laser-induced fluorescent cooling of a solid. *Nature.* **377**, 500–503 (1995).
19. Shan, X. et al. Optical tweezers beyond refractive index mismatch using highly doped upconversion nanoparticles. *Nat. Nanotechnol.* **16**, 531–537 (2021).
20. Mushtaq, A., Yang, X. & Gao, J. Unveiling room temperature upconversion photoluminescence in monolayer WSe_2. *Opt. Express.* **30**, 45212–45220 (2022).
21. Meng, F., Yang, X. & Gao, J. Phonon-assisted upconversion photoluminescence of monolayer MoS_2 at elevated temperatures. *Opt. Express.* **31**, 28437–28443 (2023).
22. Meng, F., Yang, X. & Gao, J. High-temperature phonon-assisted upconversion photoluminescence of monolayer WSe_2. *Appl. Phys. Lett.* **123**, (2023).

23. Chu, Z. et al. Energy-resolved photoconductivity mapping in a monolayer–bilayer WSe_2 lateral heterostructure. *Nano Lett.* **18**, 7200–7206 (2018).
24. Żuberek, E. et al. Upconversion photoluminescence excitation reveals exciton–trion and exciton–biexciton coupling in hBN/WS_2/hBN Van Der Waals heterostructures. *Sci. Rep.* **12**, 13699 (2022).
25. Cong, C. et al. Anti-stokes Photoluminescence of Van Der Waals Layered Semiconductor PbI_2. *Adv. Opt. Mater.* **5**, 1700609 (2017).
26. Wu, B. et al. Uncovering the mechanisms of efficient upconversion in two-dimensional perovskites with anti-stokes shift up to 220 meV. *Sci. Adv.* **9**, eadi9347 (2023).
27. Bacher, G. et al. Exciton dynamics in In_xGa_{1-x} As/GaAs quantum-well heterostructures: competition between capture and thermal emission. *Phys. Rev. B*. **47**, 9545–9555 (1993).
28. Deutsch, Z., Neeman, L. & Oron, D. Luminescence upconversion in colloidal double quantum dots. *Nat. Nanotechnol.* **8**, 649–653 (2013).
29. Zhang, J., Li, D., Chen, R. & Xiong, Q. Laser cooling of a semiconductor by 40 kelvin. *Nature*. **493**, 504–508 (2013).
30. Mak, K. F. & Shan, J. Photonics and optoelectronics of 2D semiconductor transition metal dichalcogenides. *Nat. Photon*. **10**, 216–226 (2016).
31. Cain, J. D., Hanson, E. D., Shi, F. & Dravid, V. P. Emerging opportunities in the two-dimensional chalcogenide systems and architecture. *Curr. Opin. Solid State Mater. Sci.* **20**, 374–387 (2016).
32. Duan, X., Wang, C., Pan, A., Yu, R. & Duan, X. Two-dimensional transition metal dichalcogenides as atomically thin semiconductors: opportunities and challenges. *Chem. Soc. Rev.* **44**, 8859–8876 (2015).
33. Ahn, E. C. 2D materials for spintronic devices. *npj 2D Mater. Appl.* **4**, 17 (2020).
34. Schaibley, J. R. et al. Valleytronics in 2D materials. *Nat. Rev. Mater.* **1**, 1–15 (2016).
35. Wang, M. et al. Chemically Engineered substrates for Patternable Growth of two-dimensional Chalcogenide crystals. *ACS Nano*. **10**, 10317–10323 (2016).
36. Zhou, X., Zhang, Q., Gan, L., Li, H. & Zhai, T. Large-size growth of ultrathin SnS_2 nanosheets and high performance for phototransistors. *Adv. Funct. Mater.* **26**, 4405–4413 (2016).
37. Huang, J. K. et al. Large-area synthesis of highly crystalline WSe_2 monolayers and device applications. *ACS Nano*. **8**, 923–930 (2014).
38. Zhu, W. et al. Electronic transport and device prospects of monolayer molybdenum disulphide grown by chemical vapour deposition. *Nat. Comm.* **5**, 3087 (2014).
39. Zhou, N. et al. Narrowband spectrally selective near-infrared photodetector based on up-conversion nanoparticles used in a 2D hybrid device. *J. Mater. Chem. C*. **5**, 1591–1595 (2017).
40. Choi, W. et al. High-detectivity multilayer MoS_2 phototransistors with spectral response from Ultraviolet to Infrared. *Adv. Mater.* **24**, 5832–5836 (2012).
41. Lund, J. C. et al. Properties of lead iodide semiconductor radiation detectors. *Nucl. Instrum. Meth A*. **283**, 299–302 (1989).
42. Plekhanov, V. G. Lead halides: electronic properties and applications. *Prog Mater. Sci.* **49**, 787–886 (2004).
43. Shargaieva, O., Kuske, L., Rappich, J., Unger, E. & NickelN.H. Building blocks of Hybrid perovskites: a photoluminescence study of lead-iodide solution species. *ChemPhysChem*. **21**, 2327–2333 (2020).
44. Buin, A. et al. Materials Processing routes to trap-free Halide perovskites. *Nano Lett.* **14**, 6281–6286 (2014).
45. Zhong, M. et al. Flexible photodetectors based on phase dependent PbI_2 single crystals. *J. Mater. Chem. C*. **4**, 6492–6499 (2016).
46. Zhang, J. et al. Layered ultrathin PbI_2 single crystals for high sensitivity flexible photodetectors. *J. Mater. Chem. C*. **3**, 4402–4406 (2015).
47. Liu, X. et al. Whispering Gallery Mode Lasing from Hexagonal shaped layered lead iodide crystals. *ACS Nano*. **9**, 687–695 (2015).
48. Toulouse, A. S. et al. Frenkel-like Wannier-Mott excitons in few-layer PbI_2. *Phys. Rev. B*. **91**, 165308 (2015).
49. Du, L. et al. Perseverance of direct bandgap in multilayer 2D PbI_2 under an experimental strain up to 7.69%. *2D Mater.* **6**, 025014 (2019).
50. Frisenda, R. et al. Characterization of highly crystalline lead iodide nanosheets prepared by room-temperature solution processing. *Nanotechnology*. **28**, 455703 (2017).
51. Lin, D. Y., Guo, B. C., Dai, Z. Y., Lin, C. F. & Hsu H.-P. PbI_2 single crystal growth and its optical property study. *Crystals*. **9**, 589 (2019).
52. Yamazaki, S., Goto, T., Stokes, Anti-Stokes, D-A. & and Pair luminescences in PbI_2. *J. Phys. Soc. Jpn*. **51**, 3228–3235 (1982).
53. Ando, M. et al. Photoluminescence dynamics due to biexcitons and exciton-exciton scattering in the layered-type semiconductor PbI_2. *Phys. Rev. B*. **86**, 155206 (2012).
54. Tanaka, K., Hosoya, T., Fukaya, R. & Takeda, J. A new luminescence due to an exciton–exciton collision process in lead iodide induced by two-photon absorption. *J. Lumin.* **122**, 421–423 (2007).
55. Sears, W. M., Klein, M. L. & Morrison, J. A. Polytypism and the vibrational properties of PbI_2. *Phys. Rev. B*. **19**, 2305–2313 (1979).
56. Wangyang, P., Sun, H., Zhu, X., Yang, D. & Gao, X. Mechanical exfoliation and Raman spectra of ultrathin PbI_2 single crystal. *Mater. Lett.* **168**, 68–71 (2016).
57. Ma, H. et al. Edge Raman enhancement at layered PbI_2 platelets induced by laser waveguide effect. *Nanotechnology*. **33**, 035203 (2021).
58. Joly, A. et al. Upconversion luminescence of CdTe nanoparticles. *Phys. Rev. B*. **71**, 165304 (2005).
59. Dai, X. et al. Enhanced two-photon absorption and two-photon luminescence in monolayer MoS2 and WS2 by defect repairing. *Opt. Express*. **27**, 13744–13753 (2019).
60. Li, Q. et al. Two-photon photoluminescence and excitation spectra of InGaN/GaN quantum wells. *Appl. Phys. Lett.* **89**, 011104 (2006).
61. Tongay, S. et al. Thermally driven crossover from indirect toward direct bandgap in 2D semiconductors: $MoSe_2$ versus MoS_2. *Nano Lett.* **12**, 5576–5580 (2012).
62. O'donnell, K. P. & Chen, X. Temperature dependence of semiconductor band gaps. *Appl. Phys. Lett.* **58**, 2924–2926 (1991).
63. Golovynskyi, S. et al. Free exciton and bound excitons on pb and I vacancies and O and I substituting defects in PbI_2: photoluminescence and DFT calculations. *Appl. Surf. Sci.* **624**, 157128 (2023).
64. Lambkin, J. D., Dunstan, D. J., Homewood, K. P., Howard, L. K. & Emeny, M. T. Thermal quenching of the photoluminescence of InGaAs/GaAs and InGaAs/AlGaAs strained-layer quantum wells. *Appl. Phys. Lett.* **57**, 1986–1988 (1990).
65. Leroux, M. et al. Temperature quenching of photoluminescence intensities in undoped and doped GaN. *J. Appl. Phys.* **86**, 3721–3728 (1999).
66. Van Stryland, E. W., Woodall, M. A., Vanherzeele, H. & Soileau, M. J. Energy band-gap dependence of two-photon absorption. *Opt. Lett.* **10**, 490–492 (1985).

Acknowledgements

The authors acknowledge the support from the DARPA (W911NF2110353).

Author contributions

J. G., X. Y. and S.A. conceived the idea of the research. S.A. performed the experiments. J. G. and X. Y. directed

the research. All authors discussed the results and contributed to the manuscript.

Declarations

Competing interests
The authors declare no competing interests.

Additional information
Correspondence and requests for materials should be addressed to J.G.

Reprints and permissions information is available at www.nature.com/reprints.

Publisher's note Springer Nature remains neutral with regard to jurisdictional claims in published maps and institutional affiliations.